Supporting Information

Unveiling the Critical Role of Mn Dopant in $NiFe(OH)_2$ Catalyst for Water Oxidation

Yan Zhang[a,b], Chuan-Qi Cheng[a], Chun-Guang Kuai[a,c], Dimosthenis Sokaras[b], Xue-Li Zheng[d], Sami Sainio[b], Feng Lin[c], Cun-Ku Dong[a*], Dennis Nordlund[b*], Xi-Wen Du[a*]

[a]Institute of New-Energy Materials, School of Materials Science and Engineering, Key Laboratory for Advanced Ceramics and Machining, Technology of Ministry of Education, Tianjin University, Tianjin 300072, China.

[b]Stanford Synchrotron Radiation Light source, SLAC National Accelerator Laboratory, 2575 Sand Hill Road, Menlo Park, California, USA.

[c]Department of Chemistry, Virginia Tech, Blacksburg, VA, USA..

[d]Department of Materials Science and Engineering, Stanford University, Stanford, California, USA.

1. Experimental section

Synthesis of pure NiFe LDH. All materials were purchased from Sigma-Aldrich unless otherwise specified. All water was purified with Mill-Q Integral Water System. Pure NiFe LDH was synthesized following with previous co-precipitation method. First, 0.375 mmol nickel chloride tetrahydrate and 0.125 mmol ferrous chloride were dissolved in 200 ml ethanol and heated to 90 ℃. Then 2 mL ammonia was added dropwise into the solution followed with the addition of 50 mL distilled water. The mixture was then held at 90 ℃ for 1.5 h. Vigorous stirring with 600 $rmin^{-1}$ was applied during the synthesis. The precipitation was filtered and washed in a vacuum filter and then re-dispersed into distilled water for 30 min ultrasonication. This step was repeated for 3 times. After that the product was collected and dispensed into 30 mL deionized water for further use. The concentration of the dispersion was about 1 $mgmL^{-1}$, confirmed by ICP-MS. The product was freeze dried for XRD and Raman tests. For TEM, electrochemical and XAS test,s dispersed catalyst inks were directly used.

Synthesis of Mn-doped NiFe LDH. Mn-doped NiFe LDH was synthesized following a procedure same with that for pure sample but with additional Mn precursor. Specifically, 10 mmol manganese chloride was dissolved into 10 mL ethanol. Then 25 μL and 100 μL Mn precursor were added into the solution for preparing pure NiFe LDH so as to obtain Mn-5 and Mn-20 samples, respectively. The following steps were same with that for preparing pure sample. The final dispersed product was also 1 mg mL^{-1}, which was confirmed by ICP-MS.

Characterization. The morphology observation and element mapping characterization was conducted by JEOL 2100F TEM with an acceleration voltage of 200 kV. XRD analysis was conducted on a Bruker D8 Advance diffractometer with Cu Kα radiation and a Lynx Eye detector. Raman spectra were measured on ThermoFisher DXR Microscope with laser wavelength of 532nm and power of 4 mW. Soft XAS spectra were measured at beamline 10-1 at Stanford Synchrotron Radiation Lightsource (SSRL). The

samples loaded on CFP were used for soft XAS test. For the reference sample, chemicals were loaded directed onto the conductive double-side carbon tape. All samples were manipulated onto an aluminum stick. The total electron yield (TEY) signals were used for all samples. *Operando* hard XAS were conducted at beamline 4-1, SSRL with a home-built electrochemical cell containing a three-electrode system same with electrochemical measurement. Canberra 30-element Ge solid-state detector was used to acquire the fluorescence signal. The Ni and Fe spectra were calibrated with standard Ni and Fe foils. The *operando* chronoamperometry measurements were conducted at different bias potential on a standard electrochemical workstation (Bio-Logic SP-200). The ATHENA module implemented in the IFEFFIT software package was adopted to process the EXAFS data. Then the EXAFS fitting process was conducted with the ARTEMIS module of IFEFFIT to analyze the atoms environment.

Electrochemical test. The dispersed product with concentration of 1 mg mL^{-1} was used as the raw catalyst ink, and then 0.5 mL of the raw ink was mixed with 0.5 mL isopropanol and 20 μL Nafion solution. The mixture was dispersed uniformly with ultrasonication for 30 min to form the final catalyst ink. 36 μL of catalyst ink was carefully dropped onto a 0.3*0.3 cm^2 carbon fiber paper (CFP), with a mass loading of about 0.2 mg cm^{-2}. Then the electrode coated with catalyst was kept at room temperature until fully dried. Electrochemical test was conducted by Bio-Logic SP-300 potentiostat with a standard three-electrode system. The as-made samples were served as the work electrode with carbon electrode and Ag/AgCl electrodes as counter and reference electrodes, respectively. 1 M KOH, 0.1 M KOH and 1 M $KHCO_3$ electrolytes were prepared and purified to remove the trace Fe ion. The purification method was referred from Trotochaud et al[1]. Specifically, 2g $Ni(NO_3)_2$ $6H_2O$ was dissolved into 5mL distilled water and then added into 20mL 1M KOH to precipitate the $Ni(OH)_2$. After centrifugation and washing with distilled water and 1M KOH for three times, the acquired $Ni(OH)_2$ powder can be used to purify the solution. The powder was fully

dispersed into the solution with ultrasonication and rest for 3 hours. Then the mixture was centrifugated with 4000rpm and 15min to get the solution without Fe. After purification, the three solutions were acted as electrolyte for different pH environment. The applied potentials were converted to reversible hydrogen electrode (RHE) with the following equation:

$$E(RHE) = E(Ag/AgCl) + 0.059*pH + 0.197V \quad (S1)$$

Before recording, the potential of catalyst was scanned at 50 mV s^{-1} between 0 and 0.5 V (vs Ag/AgCl) until a stable cyclic voltammogram (CV) was obtained. Afterwards, linear sweep voltammetry (LSV) curves were recorded at the scan rates of 2 mV s-1. Then to obtain the Tafel slop, overpotential was plotted against log (J), which extracted from LSV curves.

Computational methods: All DFT calculations were performed using the Vienna Ab initio Simulation Package (VASP)[2]. The projector augmented wave (PAW)[3] pseudopotential with the PBE[4] generalized gradient approximation (GGA) exchange correlation function was utilized in the computations. All energetics of metal oxides were calculated using the DFT with the Hubbard-U framework (DFT+U) to account for strongly localized d-electrons for Ni, Fe and Mn. The Hubbard-U correction terms were at U_{eff}(Ni) = 6.45 eV, U_{eff}(Fe) = 5.3eV and U_{eff}(Mn) = 3.9 eV as obtained via linear response theory[5]. The cutoff energy of the plane wave basis set was 500 eV and a Monkhorst-Pack mesh of 9×9×5 was used in K - sampling. All structures were spin polarized and all atoms were fully relaxed with the energy convergence tolerance of 10^{-6} eV per atom, and the final force on each atom was < 0.01 eV $Å^{-1}$.

All initial structure of $Ni(OH)_2$, β-NiOOH and NiO_2 were derived from the database[6]. All the bulk structures were 2×2×2 supercells to simulate the environment in the experiment. Table S2 shows lattice constants for all optimized structures.

The Gibbs energy of formation(ΔG_f) for a metal oxides was calculated using the following equation:

$$\Delta G_f\,(NiO_xH_y) = E_{NiOxHy} - E_{Ni} - xE_O - yE_H \quad \text{(S2)}$$

Where E_{Ni} is -7.6 eV, E_O is -4.57 eV and E_H is -3.73eV[5], Fe and Mn are considered as doping elements, considering only their effect on the valence-change energy. The effect on formation energy is not considered further because it is offset during the calculation of the valence-change energy.

The change in Gibbs energy for the oxidation of Ni was calculated using the following equations:

$$\Delta G_{(Ni^{2+} \rightarrow Ni^{3+})} = \Delta G_{f(NiOOH)} - [\Delta G_{f(Ni(OH)_2} + \mu H] \quad \text{(S3)}$$

$$\Delta G_{(Ni^{3+} \rightarrow Ni^{4+})} = \Delta G_{f(NiO_2)} - [\Delta G_{f(NiOOH)} + \mu H] \quad \text{(S4)}$$

Where μH is -3.73 eV, and all calculated date are listed in Table S3.

Supplementary Figures

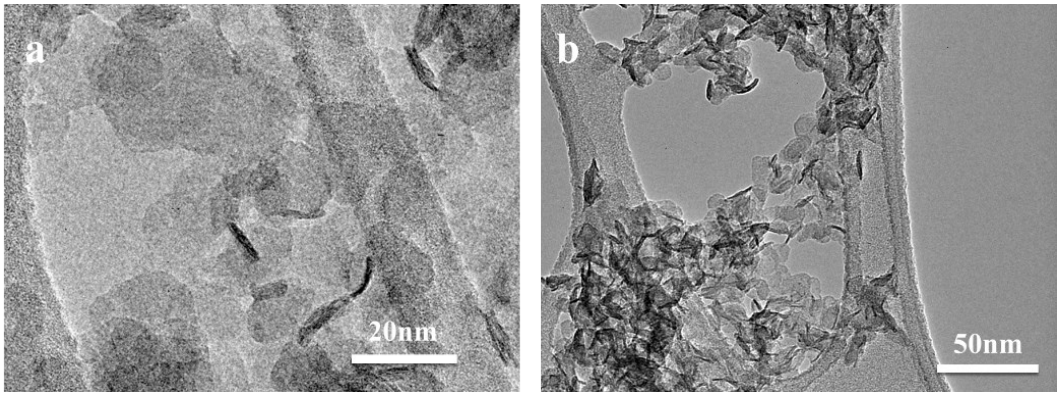

Fig S1. Low magnification TEM images of (a) pure LDH and (b) Mn-20.

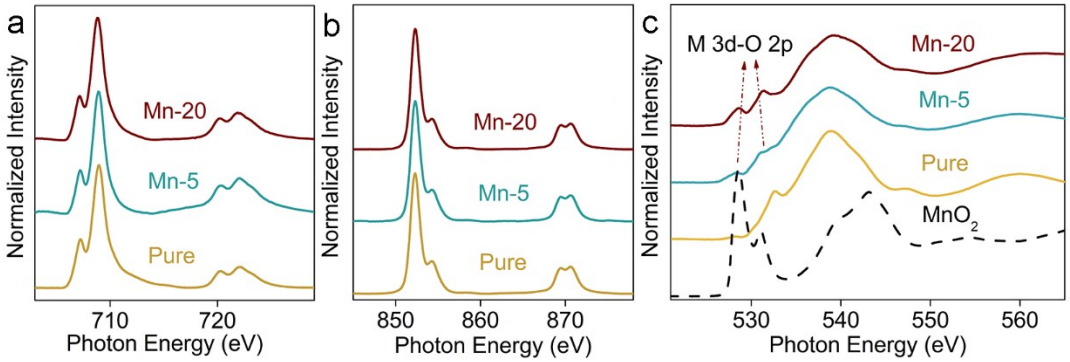

Fig S2. (a) Fe L-edge, (b) Ni L-edge and (c) O K-edge for pure LDH, Mn-5, Mn-20 samples

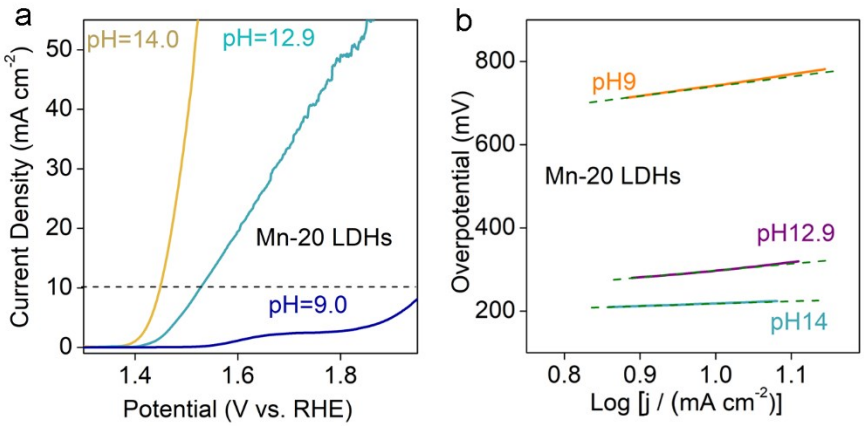

Fig S3. Electrochemistry test for Mn-20. (a) LSV in different electrolytes. (b) corresponding Tafel curves.

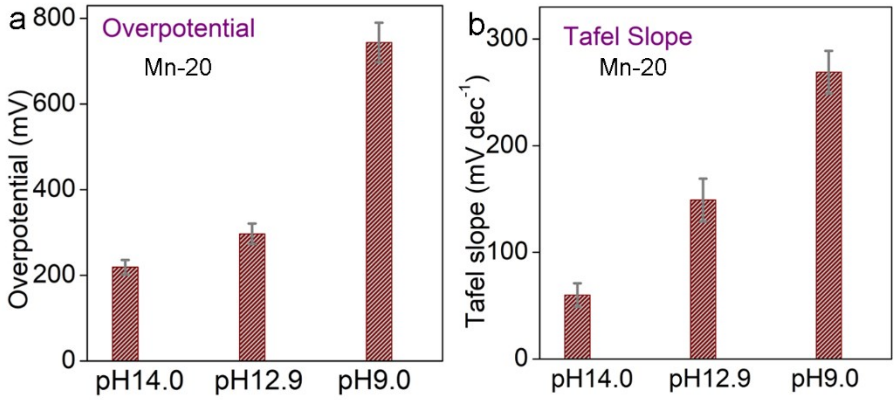

Fig S4. Comparison of overpotentials and Tafel slopes between pure LDH and Mn-20 samples

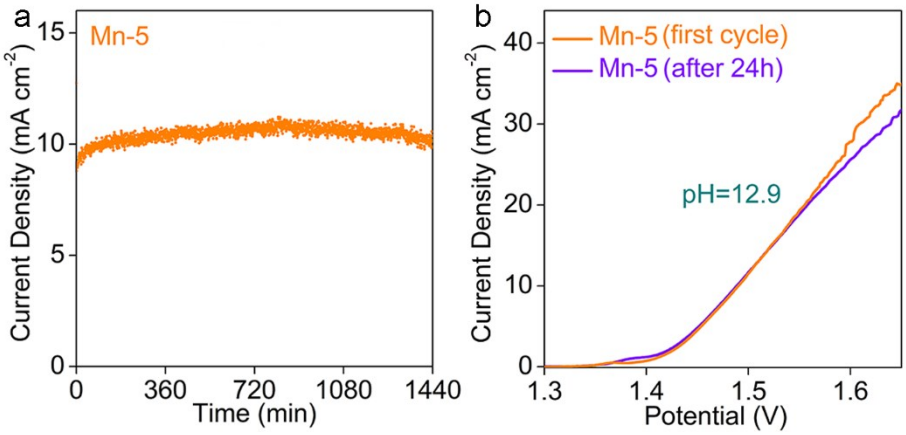

Fig S5. Stability test for Mn-5 LDH under pH=12.9. (a) chronoamperometry plot under 1.48V vs. RHE. (b) LSV curves of first cycle measurement and after chronoamperometry test.

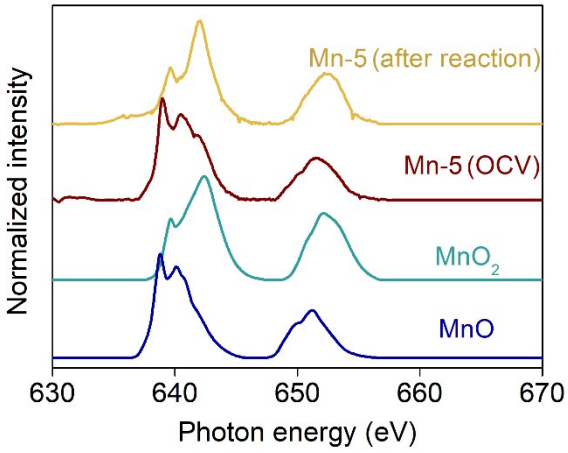

Fig S6. Mn L-edge spectra for Mn-5 before and after electrochemical measurement of 1.5V.

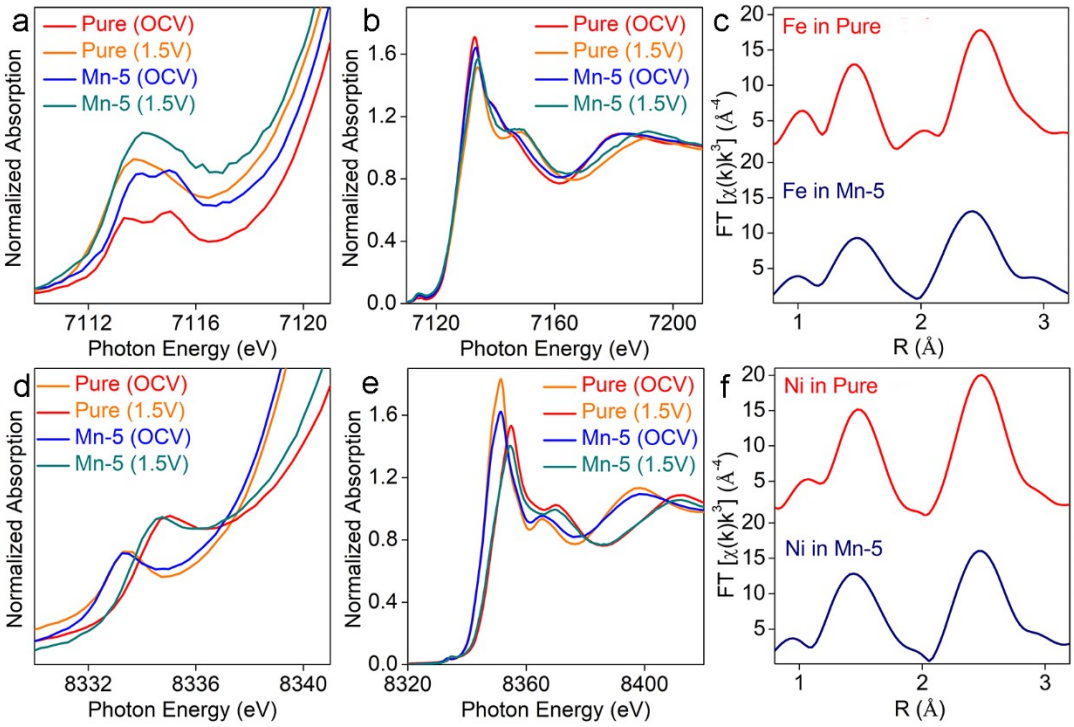

Fig S7. *In-situ* XAFS analysis during water oxidation in 1 M KOH electrolyte for pure LDH and Mn-5 under OCV and bias potential of 1.5V vs. RHE. (a) Fe K-edge pre-edge. (b) Fe near-edge range. (c) Fourier transform EXAFS analysis on Fe K edge. (d) Ni K-edge pre-edge. (e) Ni near-edge range. (f) Fourier transform EXAFS analysis on Ni K edge.

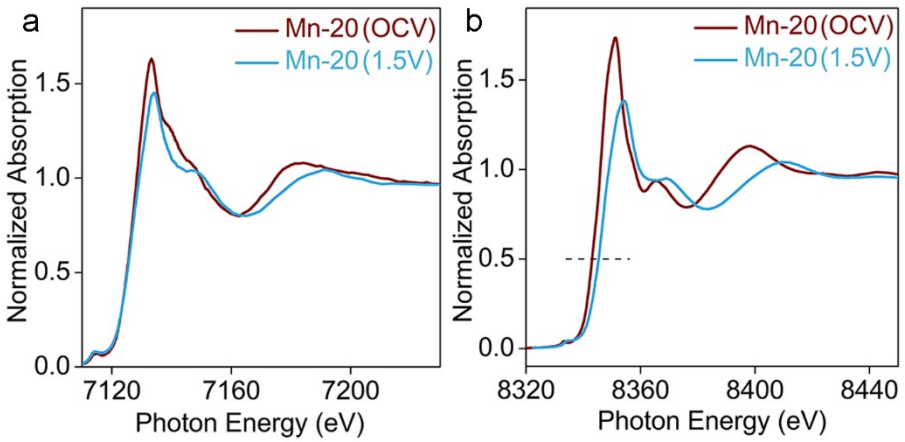

Fig S8. *In-situ* XAFS analysis during water oxidation at 0.1 M KOH for Mn-20 on (a) Fe and (b) Ni K-edge

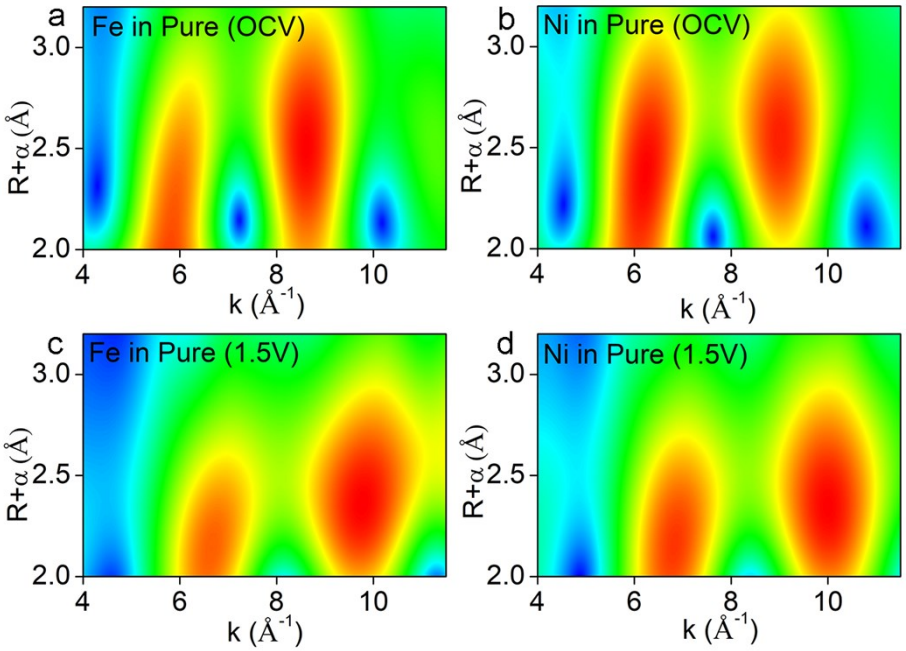

Fig S9. Wavelet transform EXAFS plots of pure LDH under OCV and bias potential of 1.5V vs. RHE in 1M KOH. (a) and (b) derivate from pure LDH without bias potential; (c) and (d) derivate from pure LDH under 1.5V vs. RHE. The Morlet parameters of the mother wavelet are κ=4; σ=1.

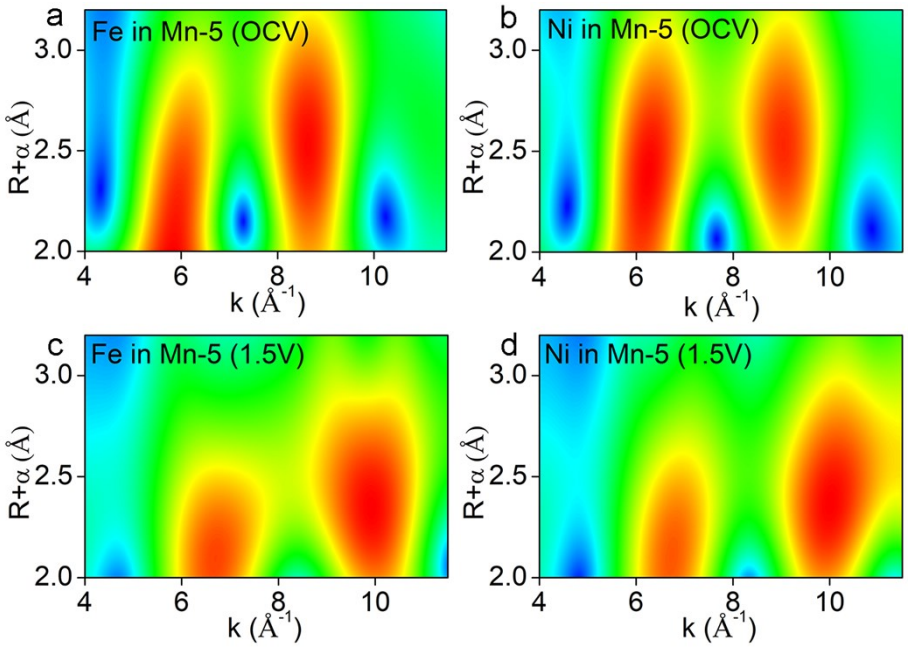

Fig S10. Wavelet transform EXAFS plots of Mn-5 under OCV and bias potential of 1.5V vs. RHE in 1M KOH. (a) and (b) derivate from Mn-5 LDH without bias potential; (c) and (d) derivate from Mn-5 LDH under 1.5V vs. RHE. The Morlet parameters of the mother wavelet are $\kappa=4$; $\sigma=1$.

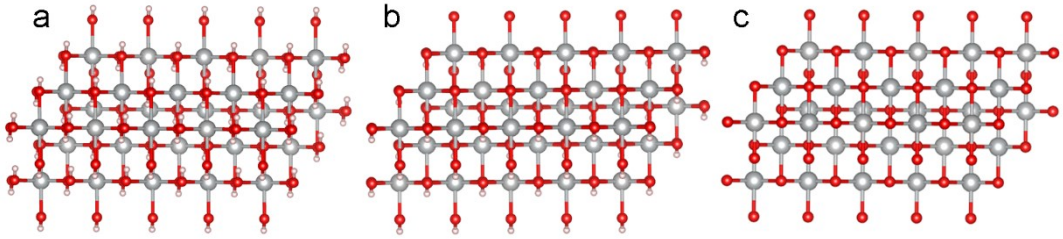

Fig S11 Optimized structures of (a) Ni hydroxide, (b) Ni oxyhydroxide, (c) Ni dioxide.

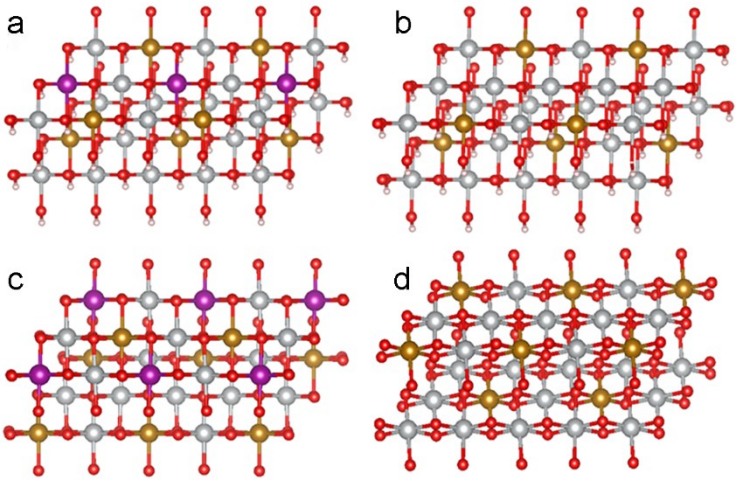

Fig S12 Optimized structures of (a) Mn-doped NiFe oxyhydroxide, (b) pure NiFe oxyhydroxide, (c) Mn-doped NiFe dioxide, (d) pure NiFe dioxide.

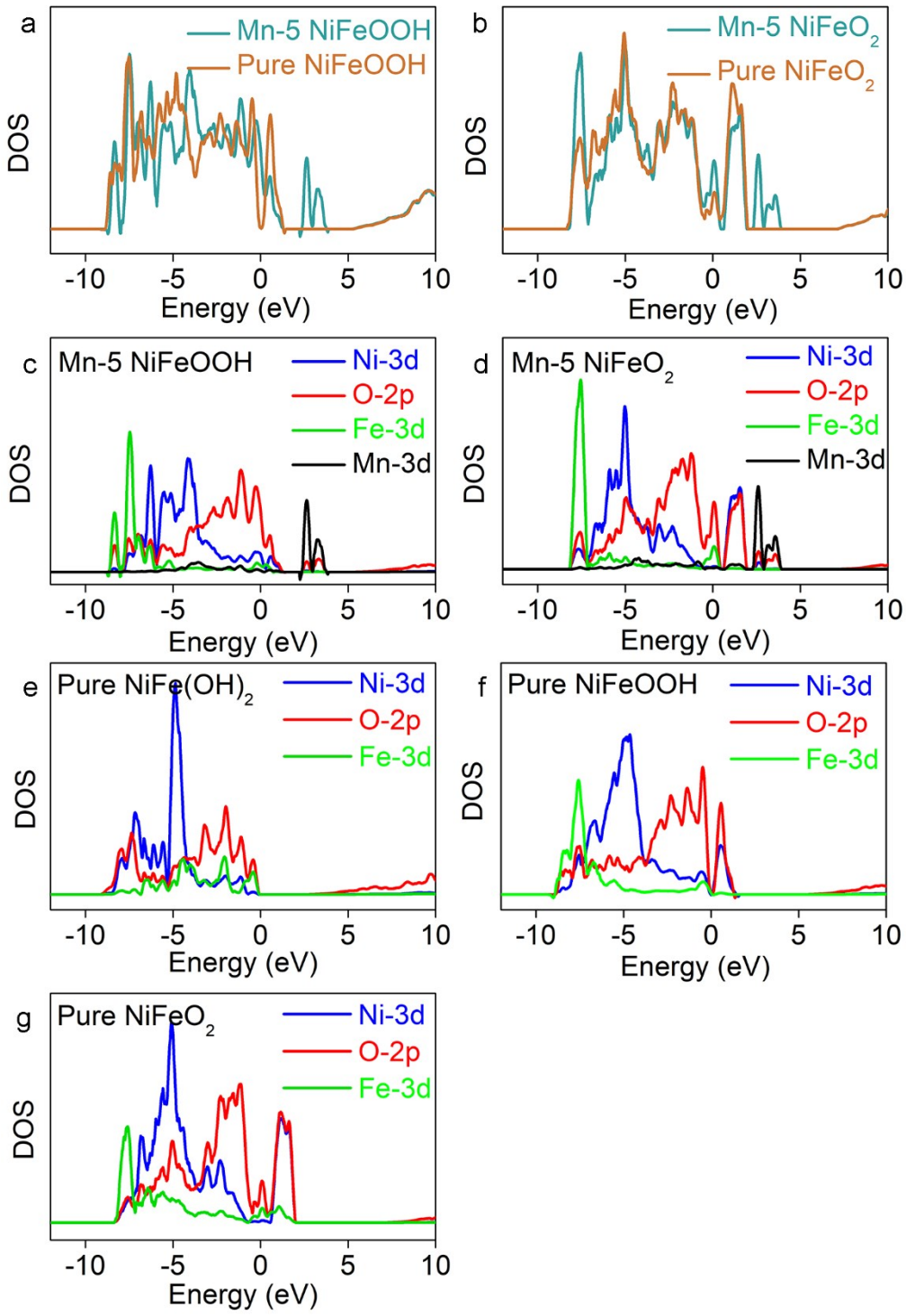

Fig S13. Density of state analysis for Ni(II) to Ni(III) to Ni(IV). (a), (b) Total Density of State (TDOS) of Mn-5 and pure NiFe oxyhydroxides and dioxides, respectively; (c), (d) Partial density of state (PDOS) corresponding to Mn-5 NiFe oxyhydroxides and dioxides, respectively. (e), (f) Partial density of state (PDOS) corresponding to pure NiFe hydroxides and dioxides, respectively.

Supplementary Tables

Table S1. EXAFS fitting results for pure and Mn-5 LDH under 1.5V vs. RHE in 0.1 M KOH electrolyte.[a]

Sample Name	Bond	CN	Distance, Å	σ^2	k-range, $Å^{-1}$	r-range, Å	R factor
Pure LDH (1.5V)	Ni-O	7.0±0.9	2.05±0.01	0.004	3-13	1-3.2	0.022
	Ni-M	7.3±1.0	3.08±0.01	0.002			
	Fe-O	6.1±0.6	2.00±0.01	0.005			0.014
	Fe-M	7.3±1.4	3.09±0.01	0.007			
Mn-5 LDH (1.5V)	Ni-O	3.3±0.4	1.89±0.01	0.004	3-13	1-3.2	0.012
	Ni-M	4.8±0.4	2.82±0.01	0.001			
	Fe-O	5.7±0.7	1.90±0.01	0.007			0.012
	Fe-M	3.2±0.5	2.83±0.01	0.002			

a. S_0^2 was fixed at 0.85.

Table S2: Lattice constants for all optimized structures.

Name	a	b	c	α	β	γ
$Ni(OH)_2$	3.14	3.21	4.68	89.74	90.27	120.76
β -NiOOH	3.00	2.82	4.84	83.15	93.61	118.00
NiO_2	2.76	2.76	5.07	90.35	89.87	120.03
$NiFe(OH)_2$	3.23	3.24	4.61	90.00	89.97	120.05
β -NiFeOOH	2.92	3.04	4.55	95.73	80.79	118.60
$NiFeO_2$	2.78	2.78	5.17	90.08	89.92	120.11
$NiFeMn(OH)_2$	3.25	3.25	4.60	90.15	89.86	120.21
β -NiFeMnOOH	3.04	3.00	4.89	108.03	91.14	119.96
$NiFeMnO_2$	2.81	2.81	5.17	89.89	90.11	119.60

Table S3: Calculated data for Gibbs free energy change.

Name	ΔG_f	$\Delta G_{(Ni^{2+} \rightarrow Ni^{3+})}$	$\Delta G_{(Ni^{3+} \rightarrow Ni^{4+})}$
$Ni(OH)_2$	-0.55		
β-NiOOH	0.87	-2.31	
NiO_2	2.56		-2.03
$NiFe(OH)_2$	-1.18		
β-NiFeOOH	-0.09	-2.64	
$NiFeO_2$	1.49		-2.15
$NiFeMn(OH)_2$	-1.35		
β-NiFeMnOOH	-0.96	-3.34	
$NiFeMnO_2$	0.61		-2.16

References

1. L. Trotochaud, S. L. Young, J. K. Ranney and S. W. Boettcher, *J. Am. Chem. Soc*, 2014, **136**, 6744-6753.
2. G. Kresse and J. Furthmüller, *Phys. Rev. B*, 1996, **54**, 11169.
3. P. E. Blöchl, *Phys. Rev. B*, 1994, **50**, 17953.
4. J. P. Perdew, K. Burke and M. Ernzerhof, *Phys. Rev. Lett*, 1996, **77**, 3865.
5. X. Zheng, B. Zhang, P. De Luna, Y. Liang, R. Comin, O. Voznyy, L. Han, F. P. G. de Arquer, M. Liu, D. Cao Thang, T. Regier, J. J. Dynes, S. He, H. L. Xin, H. Peng, D. Prendergast, X. Du and E. H. Sargent, *Nat. Chem*, 2018, **10**, 149-154.
6. A. Jain, S. P. Ong, G. Hautier, W. Chen, W. D. Richards, S. Dacek, S. Cholia, D. Gunter, D. Skinner and G. Ceder, *APL Mater*, 2013, **1**, 011002.